Available online at www.sciencedirect.com
SCIENCE DIRECT
Tetrahedron
Tetrahedron 61 (2005) 5906–5914

Supramolecular parallel β-sheet and amyloid-like fibril forming peptides using δ-aminovaleric acid residue

Arijit Banerjee,[a] Apurba Kumar Das,[a] Michael G. B. Drew[b] and Arindam Banerjee[a,*]

[a]*Department of Biological Chemistry, Indian Association for the Cultivation of Science, Jadavpur, Kolkata 700 032, India*
[b]*School of Chemistry, The University of Reading, Whiteknights, Reading RG6 6AD, UK*

Received 24 December 2004; revised 10 March 2005; accepted 23 March 2005

Abstract—Four terminally blocked tripeptides containing δ-aminovaleric acid residue self-assemble to form supramolecular β-sheet structures as are revealed from their FT-IR data. Single crystal X-ray diffraction studies of two representative peptides also show that they form parallel β-sheet structures. Self-aggregation of these β-sheet forming peptides leads to the formation of fibrillar structures, as is evident from scanning electron microscopic (SEM) and transmission electron microscopic (TEM) images. These peptide fibrils bind to a physiological dye, Congo red and exhibit a typical green-gold birefringence under polarized light, showing close resemblance to neurodegenerative disease causing amyloid fibrils.

1. Introduction

Supramolecular β-sheet forming peptides are important for their numerous potential uses in material[1] and biological[2] sciences. Self-aggregating β-sheet forming peptides sometimes provide a fibrous network to form gels.[3] Under suitable conditions, they can also provide suitable molecular scaffolds for growing neurons[2a] and cartilage.[2b]

Many fatal neurodegenerative diseases like Alzheimer's disease,[4] Parkinson's disease,[5] and prion related diseases[6] are believed to occur due to protein misfolding and subsequent protein/protein fragment aggregation to form β-sheet rich amyloid fibrils. This fact has motivated extensive research on the general mechanism of β-sheet formation and the subsequent aggregation to form fibrillar quaternary structures. Recent evidence suggests that not only disease-related proteins, but also other non-disease related proteins can be induced to form aggregated β-sheet rich amyloid fibrils under appropriate conditions.[7] Moreover, some very recent results have established that not the matured fibrils but the intermediates, that is the protofibrils, are potent neurotoxic agents for Alzheimer's disease[8] and even for prion related diseases.[9] Thorough knowledge of β-sheet aggregation is thus, important to understand the mechanism of fibrillogenesis in order to design therapeutic agents against amyloidoses. Due to non-crystallinity and extremely poor solubility of real amyloidogenic sequences, there are no significant studies that clearly demonstrate the mechanism of β-sheet formation and its aggregation at atomic resolution using single crystal X-ray diffraction studies. So, it is worthwhile to design supramolecular β-sheet forming model peptides that can form amyloid-like fibrils and are capable of forming single crystals.

It is still a controversial issue whether amyloid fibril formation proceeds preferentially through the self-assembly of parallel or antiparallel β-sheets. Recent studies have suggested that Aβ10-35 give rise to parallel[10a] β-strand whereas Aβ16-22 forms antiparallel β-strands.[10b] In our previous study, we have demonstrated that short peptides composed of non-coded amino acids can self-assemble to form amyloid-like fibril forming supramolecular parallel β-sheet structure in crystals.[11]

δ-Ava (δ-aminovaleric acid) has been used for conformational interest to design new foldamers. Previous reports described that an oligopeptide with a centrally located δ-Ava residue forms a helical conformation in solution[12a] and an octapeptide with a δ-Ava residue at the central position can form a β-hairpin structure in solution.[12b] Very recently, Baldauf et al. have demonstrated all possible helix types in oligomers of δ-amino acids (δ-peptides) and their stabilities employing various methods of ab initio MO theory.[13] However, in this paper, we report the use of the δ-aminovaleric acid residue (δ-Ava) in model terminally

Keywords: δ-Aminovaleric acid; Supramolecular parallel β-sheet; Amyloid-like fibril.
* Corresponding author. Tel.: +91 33 2473 4971; fax: +91 33 2473 2805; e-mail: bcab@mahendra.iacs.res.in

0040–4020/$ - see front matter © 2005 Elsevier Ltd. All rights reserved.
doi:10.1016/j.tet.2005.03.100

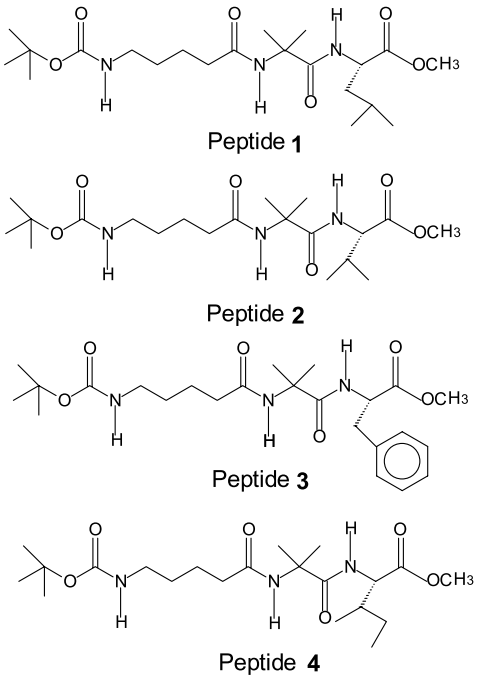

Figure 1. Schematic representation of peptides **1**, **2**, **3** and **4**.

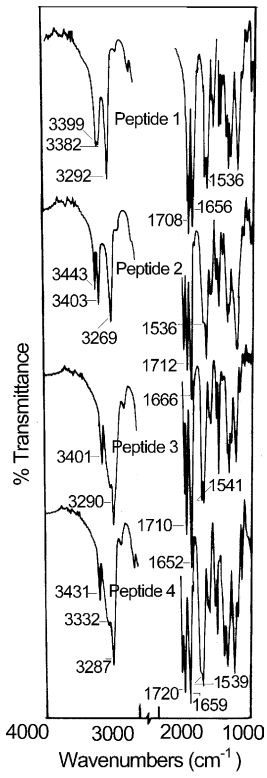

Figure 2. FT-IR spectra at the region 3000–4000 cm^{-1} (a) and 1000–2000 cm^{-1} (b) of peptides **1**, **2**, **3** and **4** in solid state.

blocked tripeptides to design and construct supramolecular β-sheet structures in the solid state and subsequent self-assembly of these β-sheets leads to the formation of amyloid-like fibrils. The schematic presentation of all terminally protected tripeptides are shown in Figure 1. To the best of our knowledge this is the first, crystallographic study of oligopeptides containing a δ-Ava residue.

2. Results and discussion

In our previous results we have demonstrated that the combination of conformationally flexible amino acid Acp (ε-aminocaproic acid) and conformationally constrained Aib (α-aminoisobutyric acid) provides overall extended structures[14] whereas by contrast a combination of conformationally flexible γ-Abu (γ-aminobutyric acid) and Aib gives a turn structure.[15] In this paper, a series of terminally blocked tripeptides containing conformationally conflicting amino acid residues (δ-aminovaleric acid and α-aminoisobutyric acid) have been designed and synthesized. The δ-aminovaleric acid residue has been used to exploit its CO and NH groups as hydrogen bonding functionalities and the centrally located tetramethylene unit provides sufficient flexibility to the peptide backbone that might help these peptides to adopt an extended backbone conformation. The conformationally restricted α-aminoisobutyric acid (Aib) residue has been used in each of the peptides to decrease conformational heterogeneity and to increase the crystallinity of the corresponding peptides. The third residues for peptides **1** and **2** are leucine (Leu) and valine (Val), respectively, having hydrophobic side chains that might help these peptides to aggregate also using van der Waals interactions. Similarly, for peptides **3** and **4** we have used Phe and Ile, respectively. Out of the four reported peptides, we obtained suitable single crystals for peptides **1** and **2** and obtained their structures. All peptides were studied using FT-IR, NMR, scanning electron microscopy, transmission electron microscopy and optical microscopy.

2.1. Solid-state FT-IR study

Preliminary information on the conformational preferences of all peptides were obtained from solid-state FT-IR studies (Fig. 2). In solid state (KBr matrix), intense bands at 3275–3375 cm^{-1} have been observed for all reported peptides indicating the presence of strongly hydrogen bonded NH groups. Important IR data of all these reported peptides are listed in Table 1. The bands corresponding to NH stretching appear over 3430 cm^{-1} suggesting the occurrence of free NH groups for peptide **2** and peptide **4**.[16] The absence of a band attributable to free NH (over 3430 cm^{-1}) indicates

Table 1. Infrared (IR) absorption frequencies (cm^{-1}) for all reported peptides in solid state (on KBr pellet)

Peptide	CO stretch (cm^{-1})	NH bend (cm^{-1})	NH stretch (cm^{-1})
Boc-δ-Ava-Aib-Leu-OMe **1**	1656 (s)	1536 (m)	3399 (m), 3382 (m), 3292 (s)
Boc-δ-Ava-Aib-Val-OMe **2**	1666 (s)	1536 (m)	3443 (m), 3403 (m), 3269 (s)
Boc-δ-Ava-Aib-Phe-OMe **3**	1652 (s)	1541 (m)	3401 (w), 3290 (s)
Boc-δ-Ava-Aib-Ile-OMe **4**	1659 (s)	1539 (m)	3431 (w), 3332 (m), 3287 (s)

s = strong, w = weak, m = medium.

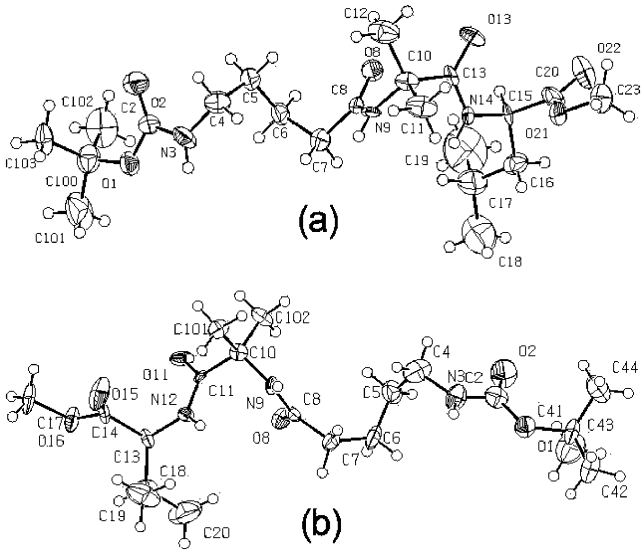

Figure 3. The ORTEP diagram of (a) peptide **1** and (b) peptide **2** with the atomic numbering scheme. Ellipsoids at 20% probability.

that all NHs are involved in intermolecular hydrogen bonding for peptides **1** and **3**.[16] The CO stretching band at around 1650–1660 cm^{-1} (amide I) and the NH bending peak near 1535 cm^{-1} (amide II) suggest the presence of intermolecularly hydrogen bonded supramolecular β-sheet-like conformations[16] for all peptides in the solid state. So, from solid-state FT-IR data it can be concluded that all the peptides share a common structural feature, the intermolecularly hydrogen-bonded sheet.

2.2. Single crystal X-ray diffraction study

These preliminary conformational data were further, supported by single crystal X-ray diffraction studies. Single crystals of peptide**1** and peptide **2** were grown from methanol–water solution. The molecular conformations of the peptides **1** and **2** in the crystals are illustrated in Figure 3. This reveals that the reported peptides are unable to form any kind of intramolecularly hydrogen bonded (N–H···O or N–H···N) turn structures despite the fact that there is a centrally positioned helicogenic Aib[17] residue for both peptides and the ϕ and ψ values of the majority of the constituent amino acid residues fall within the helical region of the Ramachandran map (Table 2 for peptide **1** and Table 3 for peptide **2**). Self-assembly of each individual monomer leads to the formation of parallel β-sheet columns along the crystallographic *a* axis (Fig. 4). For peptide **1** the parallel β-sheet column is stabilized by three intermolecular hydrogen bonds (N3–H3···O8, N9–H9···O13 and N14–H14···O22) (Table 2) exploiting all its hydrogen bonding functionalities. However, only two intermolecular hydrogen bonds (N3–H3···O8 and N9–H9···O11) are present in peptide **2** connecting individual peptide molecules to form the supramolecular parallel β-sheet column (Table 3). In peptide **2**, one N–H and one carbonyl group do not form any type of hydrogen bond. These data confirm our initial insight from the solid-state FT-IR data, that both peptides **1** and **2** possess an intermolecularly hydrogen-bonded β-sheet structure, although peptide **2** has one free NH while in peptide **1** all NHs are engaged in hydrogen-bonding. Parallel β-sheet columns self-assemble along the crystallographic *b* axis for peptide **1** (Fig. 5a) and along the

Table 2. Characteristics of peptide **1** (Boc-δ-Ava-Aib-Leu-OMe)

(a) Selected torsional angles[a] (°) of peptide **1**

Residue	ϕ	ψ	ω	θ_1	θ_2	θ_3
δ-Ava(1)	−67.14	135.37	169.55	−55.06	−69.7	−60.79
Aib(2)	−49.12	−44.92	179.26	—	—	—
Leu(3)	62.74	36.43	176.95	—	—	—

(b) Intermolecular hydrogen bonding parameters of peptide **1**

D–H···A	H···A (Å)	D···A (Å)	D–H···A (°)
N3–H3···O8[b]	2.25	3.023(10)	150
N9–H9···O13[b]	2.04	2.904(8)	179
N14–H14···O22[b]	2.53	3.358(9)	161

[a] The torsion angles for rotation about the bonds of peptide backbone: ϕ, ψ, ω. Torsions in the main chain in the N-terminal δ-Ava residue about C^{α}-C^{β}, C^{β}–C^{γ} and C^{γ}–C^{δ} θ_3 to θ_1, respectively.
[b] Symmetry element $-1+x, y, z$.

Table 3. Characteristics of peptide **2** (Boc-δ-Ava-Aib-Val-OMe)

(a) Selected torsional angles[a] (°) of peptide **2**

Residue	ϕ	ψ	ω	θ_1	θ_2	θ_3
δ-Ava(1)	80.09	−129.31	−175.43	59.27	76.26	57.75
Aib(2)	56.73	40.79	170.98	—	—	—
Val(3)	−73.76	150.88	173.46	—	—	—

(b) Intermolecular hydrogen bonding parameters of peptide **2**

D–H···A	H···A (Å)	D···A (Å)	D–H…A (°)
N3–H3···O8[b]	2.31	3.028(8)	142
N9–H9···O11[b]	2.12	2.915(6)	153

[a] The torsion angles for rotation about the bonds of peptide backbone: ϕ, ψ, ω. Torsions in the main chain in the N-terminal δ-Ava residue about C^{α}–C^{β}, C^{β}–C^{γ} and C^{γ}–C^{δ} θ_3 to θ_1, respectively.
[b] Symmetry element $-1+x, y, z$.

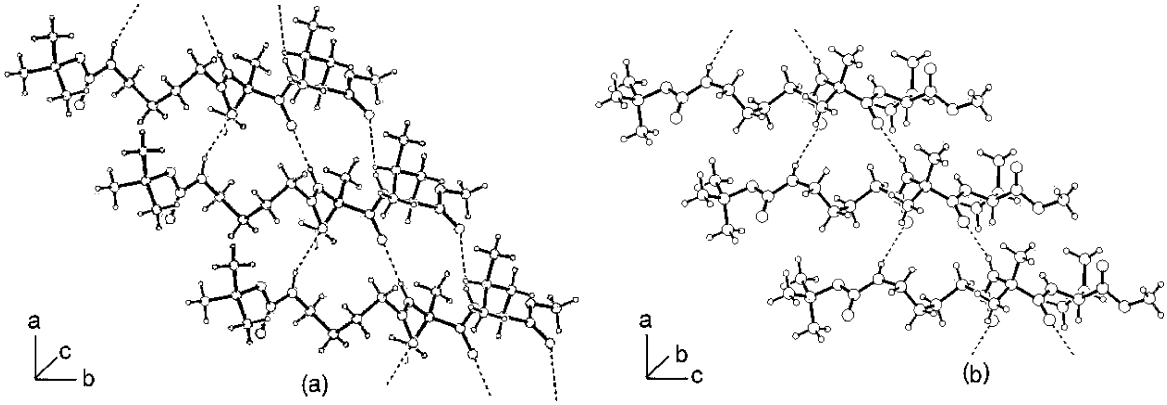

Figure 4. (a) Packing diagram of peptide **1** along *a* projection and (b) Packing diagram of peptide **2** along *a* projection illustrating intermolecular hydrogen bonding in solid state and the formation continuous β-sheet columns. Hydrogen bonds are shown as dotted lines.

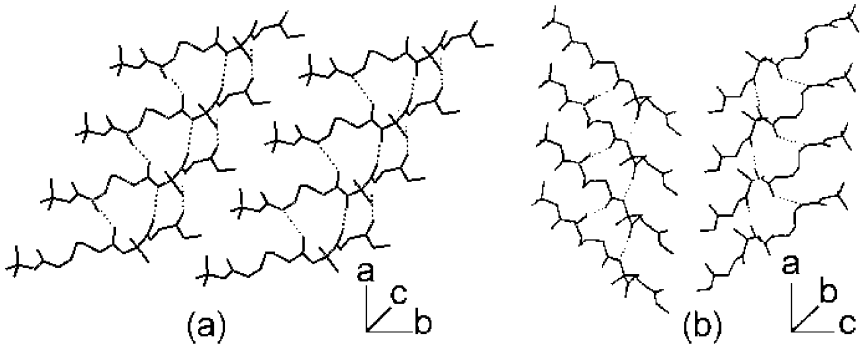

Figure 5. (a) Packing of peptide **1** along crystallographic *b* direction and (b) packing of peptide **2** along crystallographic *c* direction forming β-sheet layer structures. Hydrogen bonds are shown as dotted lines.

crystallographic *c* axis for peptide **2** (Fig. 5b) to form two-dimensional β-sheet layers. Each β-sheet layer is then regularly stacked along crystallographic *c* axis for peptide **1** (Fig. 6) and along crystallographic *b* axis for peptide **2** (Fig. 7) using van der Waals' interactions forming complex quaternary β-sheet structures. Crystal data for peptides **1** and **2** are listed in Table 4.

Except the ψ_1 for peptide **1** and ψ_1 and ψ_3 for peptide **2**, all ϕ, ψ values of these peptides **1** and **2** fall within the helical region of the Ramachandran plot (Tables 2 and 3). However, neither of these peptide backbones adopts turn or turn-like structure. No intramolecular hydrogen bond has been observed. Instead, these peptides self-aggregate to form intermolecularly hydrogen-bonded supramolecular β-sheet structures. It is also noteworthy that C–C bonds along the polymethylene units of the δ-Ava residue adopt gauche conformations. However, the overall molecular conformations of peptides **1** and **2** are flat without any noticeable bend or turn.

2.3. Scanning electron microscopic study

The morphological studies of all peptides were carried out using a scanning electron microscope (SEM). The scanning electron microscopic (SEM) images of peptides **1**, **2**, **3** and **4** (Figs. 8–11, respectively) of the dried fibrous material grown from methanol–water clearly demonstrate that the aggregates in the solid state are bunches of long small filaments, resembling amyloid fibrils.[18]

2.4. Transmission electron microscopic study

Transmission electron microscopy of all the peptides at high magnification provides information concerning their detailed structure although only a two dimensional

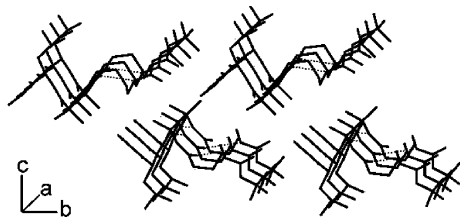

Figure 6. Higher order packing of peptide **1** along crystallographic *c* axis and forming quaternary β-sheet structures. Hydrogen bonds are shown as dotted lines.

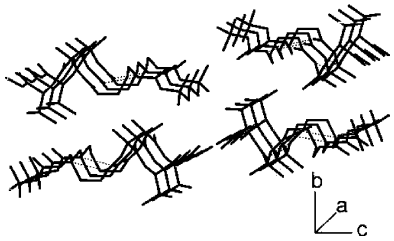

Figure 7. Higher order packing of peptide **2** along crystallographic *b* axis and forming quaternary β-sheet structures. Hydrogen bonds are shown as dotted lines.

Table 4. Crystallographic data for peptide **1** and **2**

	Peptide **1**	Peptide **2**
Formula	$C_{21}H_{39}N_3O_6$	$C_{20}H_{37}N_3O_6$
Formula weight	429.55	415.53
Crystallizing solvent	Methanol–water	Methanol–water
Crystal system	Orthorhombic	Orthorhombic
Temperature (K)	293	293
Space group	*P*212121	*P*212121
a (Å)	6.100 (8)	6.143 (8)
b (Å)	14.325 (16)	13.156 (15)
c (Å)	29.94 (3)	29.50 (3)
U (Å^3)	2616 (5)	2384 (5)
Z	4	4
*D*calcd (g cm^{-3})	1.091	1.158
λ (Å)	0.71073	0.71073
*R*1 ($I>2\sigma(I)$)	0.1050	0.0958
*wR*2 ($I>2\sigma(I)$)	0.2643	0.2041

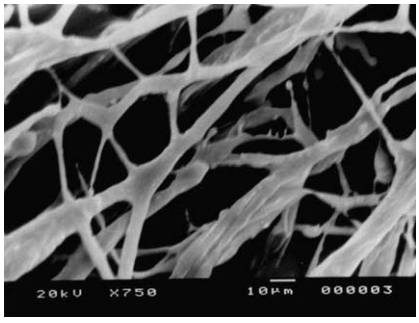

Figure 8. SEM image of dried material of peptide **1** obtained from methanol–water solution by slow evaporation.

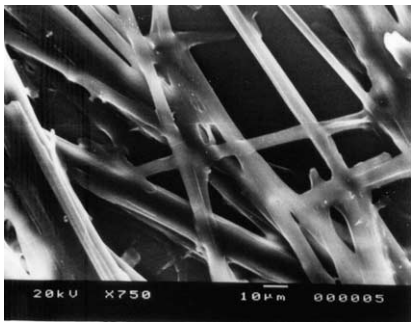

Figure 9. Typical SEM image of dried fibrous material of peptide **2** obtained from methanol–water solution by slow evaporation.

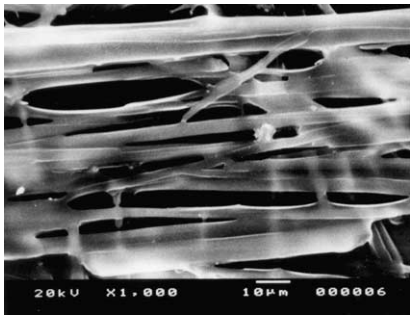

Figure 10. Typical SEM image of dried material of peptide **3** showing amyloid-like fibrillar morphology obtained from methanol–water solution by slow evaporation.

projection of the specimen could be imaged. All the peptides exhibit fibrillar morphology under the TEM. The representative TEM image of peptide **3** (Fig. 12) reveals that the peptide exists as a bunch of long unbranched filaments having diameter ~20–40 nm.

2.5. Congo red binding study

Air-dried drops of the solution of all these peptides were stained with a physiological dye Congo red and under cross polarizers these peptide fibrils exhibit green birefringence, characteristic feature of amyloid fibrils when investigated

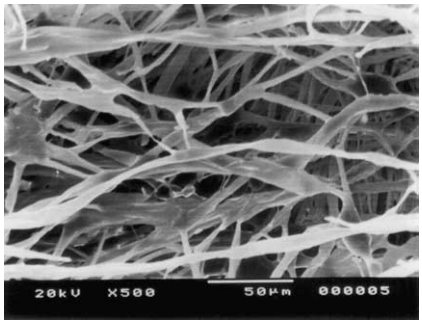

Figure 11. Typical SEM image of dried material of peptide **4** showing amyloid-like fibrillar morphology obtained from methanol–water solution by slow evaporation.

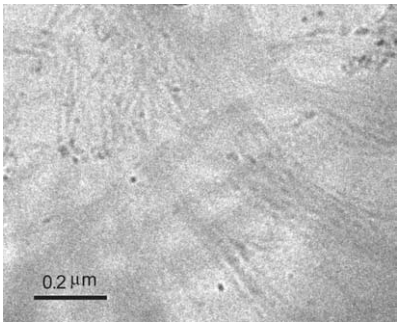

Figure 12. Transmission electron micrograph of peptide **3** showing amyloid-like morphology. The sample was prepared on a carbon coated copper grid by slow evaporation of methanol–water solution of the peptide **3**.

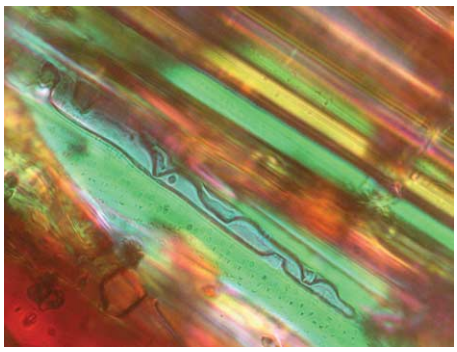

Figure 13. Congo red stained peptide **1** fibrils observed through crossed polarizers showing green-gold birefringence a characteristic feature of amyloid fibrils.

microscopically.[19] Figure 13 is a representative picture of peptide **1** stained with Congo red, and exhibits distinct green-gold birefringence under polarized light.

3. Conclusion

Solid-state FT-IR data of all peptides (peptides **1**, **2**, **3** and **4**) reveal that, all reported peptides self-associate to form intermolecularly hydrogen bonded supramolecular β-sheet structure. Crystal structures of two peptides (peptide **1** and peptide **2**) not only support the preliminary informational feature obtained from the solid-state FT-IR data but also suggest that these two peptides self-aggregate in a parallel orientation. Upon further self-assembly, these beta sheet structures produce peptide fibrils. All reported peptides show their morphological similarity with amyloidogenic proteins or protein fragments. They also bind to the physiological dye Congo red and exhibit a typical green-gold birefringence under polarized light like amyloid fibrils. Previously, it has been shown that fibril formation of Alzheimer's-associated Aβ peptide fragment proceeds via parallel β-sheet formation.[12a,20a] Some very recent results also demonstrate that fragments of Prion proteins[20b,c] and even Tau filament fragments[20d] also self-aggregate via parallel β-sheet formation. So, this study of the amyloid-like fibril forming model peptide with parallel β-sheet structure at atomic resolution may assist the scientific community studying amyloid diseases in investigating the pathway(s) and self-assembly mechanism during amyloid fibril formation. Moreover, insertion of δ-Ava residues into the peptide backbone not only helps to form hydrogen-bonded supramolecular β-sheet structures, but also provides proteolytic resistance as δ-Ava is homomorphous with the Gly-Gly segment of any peptide.

4. Experimental

4.1. Synthesis of peptides

All peptides were synthesized by conventional solution phase methods by using racemization free fragment condensation strategy.[21] The Boc group was used for N-terminal protection and the C-terminus was protected as a methyl ester. Deprotections were performed using the saponification method. Couplings were mediated by dicyclohexylcarbodiimide/1-hydroxybenzotriazole (DCC/HOBt). All the intermediates were characterized by ^{1}H NMR (300 MHz) and thin layer chromatography (TLC) on silica gel and used without further purification. The final products were purified by column chromatography using silica (100–200 mesh size) gel as stationary phase and ethyl acetate/ethyl acetate–toluene mixture as eluent. The purified final compounds were fully characterized by 300 MHz ^{1}H NMR spectroscopy, mass spectrometry and elemental analysis.

4.1.1. Boc-δ-Ava-OH 5. A solution of δ-aminovaleric acid (3.51 g, 30 mmol) in a mixture of dioxane (60 mL), water (30 mL) and 1 M NaOH (60 mL) was stirred and cooled in an ice-water bath. Di-*tert*-butylpyrocarbonate (7.2 g, 33 mmol) was added and stirring was continued at room temperature for 6 h. Then the solution was concentrated in vacuo to about 30–40 mL, cooled in an ice water bath, covered with a layer of ethyl acetate (about 50 mL) and acidified with a dilute solution of $KHSO_4$ to pH 2–3 (Congo red). The aqueous phase was extracted with ethyl acetate and this operation was done repeatedly. The ethyl acetate extracts were pooled, washed with water and dried over anhydrous Na_2SO_4 and evaporated concentrated in vacuo. The pure material **5** was obtained as a waxy solid. Yield=5.6 g (25.8 mmol, 86%); δ_H (300 MHz, CD_3SOCD_3) 11.76 (–COOH, 1H, br), 6.54 (δ-Ava(1) NH, 1H, t, J=9 Hz), 2.64–2.70 (δ-Ava(1) C^{δ}Hs, 2H, m), 1.94–1.99 (δ-Ava(1) C^{α}Hs, 2H, m), 1.21–1.26 (δ-Ava(1) C^{β} and C^{γ} Hs, 4H, m), 1.14 (Boc-CH_3, 9H, s); mass spectral (ESI) data $(M+Na)^+$=240.1, M_{calcd}=217; (found: C, 55.35; H, 8.72; N, 6.42 $C_{10}H_{19}N_1O_4$ (217) requires C, 55.30; H, 8.76; N, 6.45%).

4.1.2. Boc-δ-Ava(1)-Aib(2)-OMe 6. Boc-δ-Ava-OH (5.4 g, 25 mmol) was dissolved in dichloromethane (DCM) (50 mL) in an ice-water bath. H-Aib-OMe was isolated from the corresponding methyl ester hydrochloride (7.67 g, 50 mmol) by neutralization, subsequent extraction with ethyl acetate and concentration to 15 mL and this was added to the reaction mixture, followed immediately by dicyclohexylcarbodiimide (DCC) (5.15 g, 25 mmol). The reaction mixture was allowed to come to room temperature and stirred for 48 h. DCM was evaporated, the residue was dissolved in ethyl acetate (60 mL), and dicyclohexylurea (DCU) was filtered off. The organic layer was washed with 2 M HCl (3×50 mL), brine (2×50 mL), then 1 M sodium carbonate (3×50 mL) and brine (2×50 mL) and dried over anhydrous sodium sulfate, and evaporated in vacuo to yield Boc-δ-Ava-Aib-OMe **6** as a white solid. Yield=6.68 g (21.14 mmol, 84.5%); mp 104–106 °C; δ_H (300 MHz, $CDCl_3$) 6.24 (Aib(2) NH, 1H, s), 4.72 (δ-Ava(1) NH, 1H, t, J=9.6 Hz), 3.73 (–OCH_3, 3H, s), 3.14–3.10 (δ-Ava(1) C^{δ}Hs, 2H, m), 2.17–2.22 (δ-Ava(1) C^{α}Hs, 2H, m), 1.60–1.71 (δ-Ava(1) C^{β} and C^{γ}Hs, 4H, m), 1.53 (Aib(2) C^{β}Hs, 6H, s), 1.44 (Boc-CH_3s, 9H, s); mass spectral (ESI) data $(M+Na)^+$=339.2, M_{calcd}=316; (found: C, 56.93; H, 8.82; N, 8.92 $C_{15}H_{28}N_2O_5$ (316) requires C, 56.96; H, 8.86; N, 8.86%).

4.1.3. Boc-δ-Ava(1)-Aib(2)-OH 7. To a sample of **6** (6.64 g, 21 mmol), MeOH (75 mL) and 2 M NaOH (30 mL) were added and the progress of saponification

was monitored by thin layer chromatography (TLC). The reaction mixture was stirred. After 10 h. methanol was removed in vacuo, the residue was dissolved in water (50 mL), and washed with diethyl ether (2×50 mL). Then the pH of the aqueous layer was adjusted to 2 using 1 M HCl and it was extracted with ethyl acetate (3×50 mL). The extracts were pooled, dried over anhydrous sodium sulfate, and evaporated in vacuo to yield compound **7** as a white solid. Yield=6.08 g (20.13 mmol, 95.86%); mp 122–124 °C; δ_H (300 MHz, CD_3SOCD_3) 12.18 (–COOH, 1H, br), 7.89 (Aib(2) NH, 1H, s), 6.71 (δ-Ava(1) NH, 1H, t, J= 8.7 Hz), 3.89–3.97 (δ-Ava(1) C^{δ}Hs, 2H, m), 1.52–1.61 (δ-Ava(1) C^{α}Hs, 2H, m), 1.28–1.35 (δ-Ava(1) C^{β} and C^{γ}Hs, 4H, m), 1.13 (Boc-CH_3, 9H, s), 0.81 (Aib (2) C^{β}Hs, 6H, s); mass spectral (ESI) data $(M+Na)^+$=325.2, M_{calcd}=302; (found: C, 55.65; H, 8.58; N, 9.31. $C_{14}H_{26}N_2O_5$ (302) requires C, 55.63; H, 8.61; N, 9.27%).

4.1.4. Boc-δ-Ava(1)-Aib(2)-Leu(3)-OMe 1. Boc-δ-Ava-Aib-OH **7** (1.51 g, 5 mmol) was dissolved in DMF (10 mL) in an ice-water bath. H-Leu-OMe was isolated from methyl ester hydrochloride (1.82 g, 10 mmol) by neutralization, subsequent extraction with ethyl acetate and concentration to 7 mL and it was added to the reaction mixture, followed immediately by dicyclohexylcarbodiimide (DCC) (1.03 g, 5 mmol) and HOBt (0.68 g, 5 mmol). The reaction mixture was allowed to come to room temperature and stirred for 72 h. The residue was taken in ethyl acetate (30 mL), and dicyclohexylurea (DCU) was filtered off. The organic layer was washed with 2 M HCl (3×30 mL), brine (2×30 mL), then 1 M sodium carbonate (3×30 mL) and brine (2×30 mL) and dried over anhydrous sodium sulfate and evaporated in vacuo to yield **1** (1.59 g) in form of white solid. Purification was done by silica gel column (100–200 mesh) using ethyl acetate as eluent.

Yield=1.59 g (3.7 mmol, 74%); mp 114–116 °C; δ_H (300 MHz, $CDCl_3$) 7.07 (Leu(3) NH, 1H, d, J=7.5 Hz), 6.18 (Aib(2) NH, 1H, s), 4.76 (δ-Ava(1) NH, 1H, t, J= 7.15 Hz), 4.60–4.53 (Leu(3) C^{α}H, 1H, m), 3.73 (-OCH_3, 3H, s), 3.14–3.12 (δ-Ava(1) C^{δ}Hs, 2H, m), 2.25–2.20 (δ-Ava(1) C^{α} Hs, 2H, m), 1.86–1.82 (Leu(3) C^{β}Hs, 2H, m), 1.68–1.62 (δ-Ava(1) C^{β} Hs and C^{γ}Hs, 4H, m), 1.58 (Aib(2) C^{β}Hs, 3H, s), 1.56 (Aib(2) C^{β}Hs, 3H, s), 1.54–1.49 (Leu(3) C^{γ}H 1H, m), 1.44 (Boc-CH_3, 9H, s), 0.96–0.91 (Leu(3) C^{δ}Hs, 6H, m); mass spectral (ESI) data $(M+H)^+$=430.4, M_{calcd}= 429; $[\alpha]_D^{24.9}$ +6.39 (c 2.12, $CHCl_3$); (found: C, 58.78; H, 9.07; N, 9.83 $C_{21}H_{39}N_3O_6$ (429) requires C, 58.74; H, 9.1; N, 9.79%).

4.1.5. Boc-δ-Ava(1)-Aib(2)-Val(3)-OMe 2. A sample of **7** (1.51 g, 5 mmol) in DMF (10 mL) was cooled in an ice water bath. H-Val-OMe was isolated from of the corresponding methyl ester hydrochloride (1.68 g, 10 mmol) by neutralization, subsequent extraction with ethyl acetate and concentration to 7 mL and this was added to the reaction mixture, followed immediately by DCC (1.03 g, 5 mmol) and HOBt (0.68 g, 5 mmol). The reaction mixture was stirred for 3 days. The residue was taken in ethyl acetate (50 mL) and DCU was filtered off. The organic layer was washed with 2 M HCl (3×50 mL), brine (2×50 mL), 1 M sodium carbonate (3×50 mL), brine (2×50 mL), dried over anhydrous sodium sulfate and evaporated in vacuo to yield white solid of **2**. Purification was done by silica gel column using ethyl acetate as eluent. Yield=1.5 g (3.6 mmol, 72%); mp 110–112 °C; δ_H (300 MHz, $CDCl_3$) 7.13 (Val(3) NH, 1H, d, J=8.1 Hz), 6.10 (Aib(2) NH, 1H, s), 4.70 (δ-Ava(1) NH, 1H, br), 4.48–4.52 (Val(3) C^{α}H, 1H, m), 3.73 (–OCH_3, 1H, s), 3.15–3.11 (δ-Ava(1) C^{δ}Hs, 2H, m), 2.25–2.21 (δ-Ava(1) C^{α}Hs, 2H, m), 2.18–2.16 (Val C^{β}H, 1H, m), 1.63–1.71 (δ-Ava(1) C^{β} and C^{γ}Hs, 4H, m and 1H, m), 1.43 (Boc-CH_3, 9H, s), 1.25 (Aib(2) C^{β}Hs, 6H, s), 0.96–0.88 (Val(3) C^{γ}Hs, 6H, m); Mass spectral (ESI) data $(M+H)^+$=416.4, M_{calcd}=415; $[\alpha]_D^{25}$ +17.4 (c 2.16, $CHCl_3$); (found: C, 57.87; H, 8.95; N, 10.07; $C_{20}H_{37}N_3O_6$ (415) requires C, 57.83; H, 8.92; N, 10.12%).

4.1.6. Boc-δ-Ava(1)-Aib(2)-Phe(3)-OMe 3. Boc-δ-Ava(1)-Aib(2)-OH (1.51 g, 5 mmol) in DMF (10 mL) was cooled in an ice-water bath and H-Phe-OMe was isolated from the corresponding methyl ester hydrochloride (2.16 g, 10 mmol) by neutralization, subsequent extraction with ethyl acetate and concentration to 7 mL and it was added to the reaction mixture, followed immediately by DCC (1.03 g, 5 mmol) and of HOBt (0.68 g, 5 mmol). The reaction mixture was stirred for three days. The residue was taken in ethyl acetate (60 mL) and the DCU was filtered off. The organic layer was washed with 2 M HCl (3× 50 mL), brine (2×50 mL), 1 M sodium carbonate (3× 50 mL), brine (2×50 mL), dried over anhydrous sodium sulfate and evaporated in vacuo to yield **3** as white solid. Purification was done by silica gel column (100–200 mesh) using ethyl acetate as eluent. Yield=1.67 g (3.6 mmol, 72%); mp 117–119 °C; δ_H (300 MHz, $CDCl_3$) 7.11–7.33 (Ph ring protons of Phe(3), 5H, m), 6.88 (Phe(3) NH, 1H, d, J=7.26 Hz), 6.05 (Aib(2) NH, 1H, s), 4.86–4.80 (Phe(3) C^{α}H, 1H, m), 4.70 (δ-Ava(1) NH, 1H, m), 3.73 (–OCH_3, 3H, s), 3.21–3.06 (Phe(3) C^{β}Hs, 2H, m and δ-Ava(1) C^{δ}Hs, 2H, m), 2.20–2.09 (δ-Ava(1) C^{α}Hs, 2H, m), 1.66–1.59 (δ-Ava(1) C^{β} and C^{γ}Hs, 4H, m), 1.49 (Aib(2) C^{β} Hs, 6H, s), 1.43 (Boc-CH_3, 9H, s); mass spectral (ESI) data $(M+Na)^+$=486.2, M_{calcd}=463; $[\alpha]_D^{25.1}$ +36.91 (c 2.25, $CHCl_3$); (found: C, 62.27; H, 8.12; N, 9.02. $C_{24}H_{37}N_3O_6$ (463) requires C, 62.20; H, 7.99; N, 9.07%).

4.1.7. Boc-δ-Ava(1)-Aib(2)-Ile(3)-OMe 4. Boc-δ-Ava-Aib-OH (1.51 g, 5 mmol) was dissolved in DMF (10 mL) in an ice-water bath. H-Ile-OMe was isolated from methyl ester hydrochloride (1.82 g, 10 mmol) by neutralization, subsequent extraction with ethyl acetate and concentration to 7 mL and it was added to the reaction mixture, followed immediately by dicyclohexylcarbodiimide (DCC) (1.03 g, 5 mmol) and HOBt (0.68 g, 5 mmol). The reaction mixture was allowed to come to room temperature and stirred for 72 h. The residue was taken in ethyl acetate (30 mL), and dicyclohexylurea (DCU) was filtered off. The organic layer was washed with 2 M HCl (3×30 mL), brine (2×30 mL), then 1 M sodium carbonate (3×30 mL) and brine (2× 30 mL) and dried over anhydrous sodium sulfate and evaporated in vacuo to yield **4** as white solid. Purification was done by silica gel column (100–200 mesh) using ethyl acetate as eluent. Yield =1.58 g (3.68 mmol, 73.6 %); mp 108–110 °C; δ_H (300 MHz, $CDCl_3$) 7.18 (Ile(3) NH, 1H, d, J=8.1 Hz), 6.25 (Aib(2) NH, 1H, s), 4.77 (δ-Ava(1) NH, 1H, m), 4.62–4.51 (Ile(3) C^{α}H, 1H, m), 3.73 (–OCH_3, 3H, s), 3.19–3.06 (δ-Ava(1) C^{δ}Hs, 2H, m), 2.29–2.21 (δ-Ava(1)

C^{α}Hs, 2H, m), 1.97–1.88 (Ile C^{β}Hs,1H, m), 1.70–1.62 (δ-Ava(1) C^{β} and C^{γ}Hs, 4H, m), 1.58 (Aib(2) C^{β}Hs, 3H, s), 1.55 (Aib(2) C^{β}Hs, 3H, s), 1.44 (Boc-CH_3, 9H, s), 1.24–1.11 (Ile(3) C^{γ}Hs, 2H, m), 0.99–0.90 (Ile(3) C^{γ} and C^{δ}Hs, 6H, m); Mass spectral (ESI) data $(M+Na)^+ = 452.2$, $M_{calcd} = 429$; $[\alpha]_D^{25.3} +21.35$ (*c* 2.04, $CHCl_3$); (found: C, 58.68; H, 9.13; N, 9.76. $C_{21}H_{39}N_3O_6$ (429) requires C, 58.74; H, 9.1; N, 9.79).

4.2. NMR experiments

All NMR studies were carried out on a Brüker DPX 300 MHz spectrometer at 300 K. Peptide concentrations were in the range 1–10 mM in $CDCl_3$ and CD_3SOCD_3.

4.3. FT-IR spectroscopy

The FT-IR spectra were taken using Shimadzu (Japan) model FT-IR spectrophotometer. The solid-state FT-IR measurements were performed using the KBr disk technique.

4.4. Scanning electron microscopic study

Morphologies of all reported tripeptides were investigated using optical microscopy and scanning electron microscopy (SEM). For the SEM study, fibrous materials (slowly grown from methanol–water mixtures) were dried and gold coated. Then the micrographs were taken in a SEM apparatus (Jeol Scanning Microscope-JSM-5200).

4.5. Transmission electron microscopic study

The morphologies of the reported compounds were investigated using transmission electron microscopy (TEM). The transmission electron microscopic studies of all the peptides were carried out using a small amount of the solution of the corresponding compounds on carbon-coated copper grids (200 mesh) by slow evaporation and allowed to dry in vacuum at 30 °C for two days. Images were taken at an accelerating voltage of 200 kV. TEM was performed using a JEM-2010 electron microscope.

4.6. Congo red binding study

An alkaline saturated Congo red solution was prepared. The peptide fibrils were stained by alkaline Congo red solution (80% methanol/ 20% glass distilled water containing 10 μL of 1% NaOH) for 2 min and then the excess stain (Congo red) was removed by rinsing the stained fibril with 80% methanol/20% glass distilled water solution for several times. The stained fibrils were dried in vacuum at room temperature for 24 h, then visualized at 100× or 500× magnification and birefringence was observed between crossed polarizers.

4.7. Single crystal X-ray diffraction study

For peptides**1** and **2**, single crystals were obtained from methanol–water solution by slow evaporation. Crystal data for both peptides were collected on a Marresearch Image Plate with Mo Kα radiation. The crystals were positioned at 70 mm from the Image Plate. Hundred frames were measured at 2° intervals with a counting time of 2 min. Data analyses were carried out with the XDS program.[22] The structures were solved using direct methods with the Shelx86 program.[23] Non-hydrogen atoms were refined with anisotropic thermal parameters. The hydrogen atoms bonded to carbon were included in geometric positions and given thermal parameters equivalent to 1.2 times those of the atom to which they were attached. The structures were refined on F^2 using Shelxl.[24] Crystallographic data have been deposited at the Cambridge Crystallographic Data Center references CCDC 258126, 258127 for peptides **1** and **2**.

4.8. Mass spectrometry

Mass spectra were recorded on a Hewlett Packard Series 1100MSD mass spectrometer by positive mode electrospray ionization.

Acknowledgements

We thank EPSRC and the University of Reading, U.K. for funds for the Image Plate System. This research is also supported by a grant from Department of Science and Technology (DST), India [Project No. SR/S5/OC-29/2003].

References and notes

1. (a) Aggeli, A.; Boden, N.; Cheng, Y.; Findlay, J. B. C.; Knowles, P. F.; Kovatchev, P.; Turnbull, P. J. H. *Biochemistry* **1996**, *35*, 16213–16221. (b) Scheibel, T.; Parthasarathy, R.; Sawicki, G.; Lin, X.-M.; Jaeger, H.; Lindquist, S. *Proc. Natl. Acad. Sci. U.S.A.* **2003**, *100*, 4527–4532.
2. (a) Holmes, T. C.; Lacalle, S. D.; Su, X.; Liu, G.; Rich, A.; Zhang, S. *Proc. Natl. Acad. Sci. U.S.A.* **2000**, *97*, 6728–6733. (b) Kisiday, J. D.; Jin, M.; Kurz, B.; Huang, H.; Semino, C. E.; Zhang, S.; Grodzinsky, A. J. *Proc. Natl. Acad. Sci. U.S.A.* **2002**, *99*, 9996–10001. (c) Wang, W.; Hect, M. H. *Proc. Natl. Acad. Sci. U.S.A.* **2002**, *99*, 2760–2765.
3. Aggeli, A.; Bell, M.; Boden, N.; Keen, J. N.; Knowles, P. F.; Mcleish, T. C. B.; Pitkeathly, M.; Radford, S. E. *Nature* **1997**, *386*, 259–262.
4. (a) Taubes, G. *Science* **1996**, *271*, 1493–1495. (b) Lansbury, P. T., Jr. *Acc. Chem. Res.* **1996**, *29*, 317–321. (c) Rochet, J. C.; Lansbury, P. T., Jr. *Curr. Opin. Struct. Biol.* **2000**, *10*, 60–68. (d) Walsh, D. M.; Lomakin, A.; Benedek, G. B.; Condron, M. M.; Teplow, D. B. *J. Biol. Chem.* **1997**, *272*, 22364–22372. (e) Walsh, D. M.; Hartley, D. M.; Kusumoto, Y.; Fezoui, Y.; Condron, M. M.; Lomakin, A.; Benedek, G. B.; Selkoe, D. J.; Teplow, D. B. *J. Biol. Chem.* **1999**, *274*, 25945–25952.
5. (a) Goedert, M.; Spillntini, M. G.; Davies, S. W. *Curr. Opin. Neurobiol.* **1998**, *8*, 619–632. (b) Baba, M.; Nakajo, S.; Tu, P. H.; Tomita, T.; Nakaya, K.; Lee, V. M.-Y.; Trojanowski, J. Q.; Iwatsubo, T. *Am. J. Pathol.* **1998**, *52*, 879–884. (c) Spillantini, M. G.; Crowther, R. A.; Jakes, R.; Hasegawa, M.; Goedert, M. *Proc. Natl. Acad. Sci. U.S.A.* **1998**, *95*, 6469–6473.
6. (a) Pan, K. M.; Baldwin, M.; Nguyen, J.; Gasset, M.; Serban, A.; Groth, D.; Mehlhorn, I.; Huang, Z.; Fletterick, R. J.;

Cohen, F. E. *Proc. Natl. Acad. Sci. U.S.A.* **1993**, *90*, 10962–10966. (b) Prusiner, S. B. *Proc. Natl. Acad. Sci. U.S.A.* **1998**, *95*, 13363–13383.
7. (a) Dobson, C. M. *Trends Biochem. Sci.* **1999**, *24*, 329–332. (b) Fändrich, M.; Fletcher, M. A.; Dobson, C. M. *Nature* **2001**, *410*, 165–166.
8. (a) Hardy, J.; Selkoe, D. J. *Science* **2002**, *297*, 353–356. (b) Klein, W. L.; Krafft, G. A.; Finch, C. E. *Trends Neurosci.* **2001**, *24*, 219–224. (c) Walsh, D. M.; Hartley, D. M.; Kusumoto, Y.; Fezoui, Y.; Condron, M. M.; Lomakin, A.; Benek, G. B.; Selkoe, D. J.; Teplow, D. B. *J. Biol. Chem.* **1999**, *274*, 25945–25952.
9. DeMaco, M. L.; Daggett, V. *Proc. Natl. Acad. Sci. U.S.A.* **2004**, *101*, 2293.
10. (a) Hou, L.; Zagorski, M. G. *Biophys. J.* **2004**, *86*, 1–2. (b) Gordon, D. J.; Balbach, J. J.; Tycko, R.; Meredith, S. C. *Biophys. J.* **2004**, *86*, 428–434.
11. Maji, S. K.; Drew, M. G. B.; Banerjee, A. *J. Chem. Soc., Chem. Commun.* **2001**, 1946–1947.
12. (a) Banerjee, A.; Pramanik, A.; Bhattacharya, S.; Balaram, P. *Biopolymers* **1996**, *39*, 769–777. (b) Shankaramma, S. C.; Singh, S. H.; Sathyamurthy, A.; Balaram, P. *J. Am. Chem. Soc.* **1999**, *121*, 5360–5363.
13. Baldauf, C.; Gunther, R.; Hoffman, H.-J. *J. Org. Chem.* **2004**, *69*, 6214–6220.
14. Banerjee, A.; Maji, S. K.; Drew, M. G. B.; Haldar, D.; Das, A. K.; Banerjee, A. *Tetrahedron* **2004**, *60*, 5935–5944.
15. Maji, S. K.; Banerjee, R.; Velmurugan, D.; Razak, A.; Fun, H. K.; Banerjee, A. *J. Org. Chem.* **2002**, *67*, 633–639.
16. (a) Toniolo, C.; Palumbo, M. *Biopolymers* **1977**, *16*, 219–224. (b) Mutter, M.; Maser, F.; Altman, K.-H.; Toniolo, C.; Bonora, G. M. *Biopolymers* **1985**, *24*, 1057–1074. (c) Chirgadze, Y. N.; Nevskaya, N. A. *Biopolymers* **1976**, *15*, 627–636. (d) Baron, M. H.; De Loze, C.; Toniolo, C.; Fasman, G. D. *Biopolymers* **1979**, *18*, 411–424. (e) Narita, M.; Ishikawa, K.; Sugasawa, H.; Doi, M. *Bull. Chem. Soc. Jpn.* **1985**, *158*, 1731–1737. (f) Moretto, V.; Crisma, M.; Bonora, G. M.; Toniolo, C.; Balaram, H.; Balaram, P. *Macromolecules* **1989**, *22*, 2939–2944.
17. Karle, I. L.; Balaram, P. *Biochemistry* **1990**, *29*, 4756–6747.
18. (a) Sipe, J. D.; Cohen, A. S. *J. Struct. Biol.* **2000**, *130*, 88–98. (b) Goldsbury, C. S.; Wirtz, S.; Müller, S. A.; Sunderji, S.; Wicki, P.; Aebi, U.; Frey, P. *J. Struct. Biol.* **2000**, *130*, 217–231.
19. (a) Kim, Y. S.; Randolph, T. W.; Manning, M. C.; Stevens, F. J.; Carpenter, J. F. *J. Biol. Chem.* **2003**, *278*, 10842–10850. (b) Taylor, D. L.; Allen, R. D.; Benditt, E. P. *J. Histochem. Cytochem.* **1974**, *22*, 1105–1112. (c) Lim, A.; Makhov, A. M.; Bond, J.; Tnouye, H.; Conmors, L. H.; Griffith, J. D.; Erickson, W. B.; Kirschner, D. A.; Costello, C. E. *J. Struct. Biol.* **2000**, *130*, 363–370. (d) Azriel, R.; Gazit, E. *J. Biol. Chem.* **2001**, *226*, 34156–34161.
20. (a) Benzinger, T. L. S.; Gregory, D. M.; Burkoth, T. S.; MillerAuer, H.; Lynn, D. G.; Botto, R. E.; Meredith, S. C. *Proc. Natl. Acad. Sci U.S.A.* **1998**, *95*, 13407–13412. (b) Kajava, A. V.; Baxa, U.; Wickner, R. B.; Steven, A. C. *Proc. Natl. Acad. Sci. U.S.A.* **2004**, *101*, 7885–7890. (c) Kuwata, K.; Matumoto, T.; Cheng, H.; Nagayama, K.; James, T. L.; Roder, H. *Proc. Natl. Acad. Sci. U.S.A.* **2003**, *100*, 14790–14795. (d) Margittai, M.; Langen, R. *Proc. Natl. Acad. Sci. U.S.A.* **2004**, *101*, 10278–10283.
21. Bodanszky, M.; Bodanszky, A. *The Practice of Peptide Synthesis*; Springer: New York, 1984; pp 1–282.
22. Kabsch, W. *J. Appl. Cryst.* **1988**, *21*, 916.
23. Sheldrick, G. M. *Acta Crystallogr. Sect. A* **1990**, *46*, 467.
24. Sheldrick, G. M. *Program for Crystal Structure Refinement*; University of Göttingen: Germany, 1993.